Journal of Civil Engineering and Architecture 11 (2017) 420-432
doi: 10.17265/1934-7359/2017.05.002

Finite Element Analysis of Polygon Shaped Shell Roof

Attia Mousa[1] and Hesham El Naggar[2]

1. Professor of Civil Engineering, University of Bahrain, Manama, Kingdom of Bahrain;

2. Professor of Civil Engineering, , Western University, London, Ontario, N6A 5B9, Canada

Abstract: A new spherical triangular finite element based on shallow shell formulation is developed in this paper. The element has six degrees of freedom at each corner node, five of which are the essential external degrees of freedom and the additional sixth is associated with the in-plane shell rotation. The displacement fields of the element satisfy the exact requirement of rigid body modes of motion. The element is based on independent strain assumption insofar as it is allowed by the compatibility equations. The element developed herein is first validated by applying it to the analysis of a benchmark problem involving a standard spherical shell with simply supported edges. The results of the analysis showed that reasonably accurate results were obtained even when modeling the shells using fewer elements compared to other shell element types. The element is then used in a finite element model to analyze polygon shaped spherical roof structures. The distribution of the various components of deflection and stress is obtained. Furthermore, the effect of introducing circular arched beams as stiffeners spanning the two diagonally opposite end corners is investigated. It is found that the stiffeners reduced the deflections and the stresses in the roof structure by considerable value.

Key words: Finite element, shell roof, polygon shape.

1. Introduction

Considerable attention has been given to applying the finite element method in the analysis of curved structures. Grafton and Strome [1] developed conical segments for the analysis of shell of revolution. Later, Jones and Strome [2] modified the method and used meridional elements which were found to lead to considerably improved results for the stresses. Curved rectangular and cylindrical shell elements were also developed (Connor and Brebbia [3], Cantin and Clough [4], and Sabir and lock [5]). However, to model a shell of spherical shape using the finite element method, triangular and rectangular spherical shell elements are needed.

Several spherical shell elements have been developed to analyze shells of spherical shape. Most notably, the higher order elements of Lindberg et al. [6], Yang [7] and Dawe [8] have resulted in an improvement of the accuracy of the results. However, this improvement is achieved at the expense of increased computational efforts and storage. Meanwhile, a simple alternative strain-based approach has been used to develop curved elements. In this approach, the exact terms representing all the rigid body modes and the displacement functions representing the element strain are determined by assuming independent strain functions insofar as it is allowed by the compatibility equations (Ashwell and Sabir [9]). This approach has been employed successfully in the development of different cylindrical, hyperbolic and conical shell elements by Sabir et al. [9-12] and by Mousa et at. [13-15]. These elements were found to yield faster convergence when compared with other available finite elements. The strain-based approach was also used to develop rectangular and triangular spherical shell elements (Sabir [16], Sabir and Djoudi [17], and Mousa [18]). These spherical elements possess only the five essential external nodal degrees of freedom at each corner node and were found to have excellent convergence.

Most spherical shell structures are supported by circular arched beams. In finite element analysis, these

Corresponding author: Attia Mousa, Ph.D., professor of civil and structural engineering; research fields: finite elements and numerical analysis. E-mail: attiamousa@hotmail.com.

beams are usually modeled using finite elements having six degrees of freedom at each end node to represent their general three dimensional forms of deformation. These six degrees of freedom are the usual five essential external degrees used in shell analysis together with a sixth representing the rotation about the normal to the shell surface. It is therefore of interest to introduce in the shell an additional degree of freedom (as a sixth degree) representing this in plane (as drilling) rotation in order to enhance the compatibility between the spherical shell and curved beam elements.

The strain based approach, also known as the Cardiff Approach, is employed in the present study to develop a triangular strain-based spherical shell element. This element has an in-plane rotation as a sixth degree of freedom. A shallow shell formulation is used to obtain the displacement fields. The element has six degrees of freedom at each of the three corners, the rigid modes are exactly represented and the straining is based on independent strains enforcing the elastic compatibility equations.

The element developed herein is first tested by applying it to the solution of a benchmark shell problem, and is then used to analyze a four-corner cross shaped roof structure. The distribution of the various components of stress and deflection is obtained. The stiffening effect of circular arched central beams on the performance of the roof is also investigated.

2. Development of Displacement Functions for the New Triangular Spherical Shell Element

2.1 Theoretical Considerations

A triangular shallow spherical shell element and the associated curvilinear coordinates are shown in Fig. 1.

For the shown system of curvilinear coordinates, the simplified strain displacement relationship for the spherical shell elements can be written as:

$$\varepsilon_x = \frac{\partial u}{\partial x} + \frac{w}{r}\ ,\ \varepsilon_y = \frac{\partial v}{\partial y} + \frac{w}{r}\ ,\ \varepsilon_{xy} = \frac{\partial u}{\partial y} + \frac{\partial v}{\partial x}$$
$$k_x = \frac{\partial^2 w}{\partial x^2}\ ,\ \ k_y = \frac{\partial^2 w}{\partial x^2},\ \ k_{xy} = -2\frac{\partial^2 w}{\partial x \partial y} \tag{1}$$

where, u, v and w are the displacements in the x, y and z axes; $\varepsilon_x, \varepsilon_y$ and ε_{xy} are the in-plane direct and shearing strains; k_x, k_y, and k_{xy} are the changes in-direct and twisting curvatures and r is the principal radii of curvatures.

The above six components of strain can be considered independent, as they are a function of the three displacements u, v and w and must satisfy three additional compatibility equations. These compatibility equations are derived by eliminating u, v and w from Eq. (1), hence, they are:

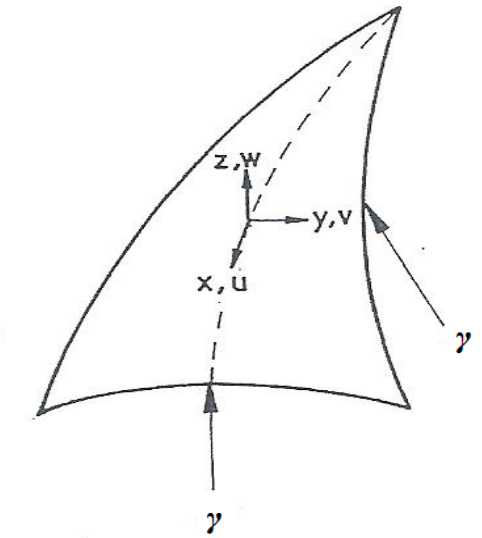

Fig. 1 Coordinate axes for triangular spherical shell element.

$$\begin{aligned}&\partial^2\varepsilon_x/\partial y^2+\partial^2\varepsilon_y/\partial x^2-\partial^2\varepsilon_{xy}/\partial x\partial y+k_x/r+k_y/r=0\\&\partial^2 k_{xy}/\partial x-2\partial k_x/\partial y=0\\&\partial k_{xy}/\partial y-2\partial k_y/\partial x=0\end{aligned}\tag{2}$$

In order to keep the element as simple as possible and to avoid the difficulties associated with internal non-geometric degrees of freedom, the developed element should possess six degrees of freedom at each of the four corner nodes: u, v, w, θx, θy and ϕ. Thus, the shape functions for a rectangular element should contain 24 independent constants.

To obtain the displacement fields due to rigid body movements, all the six strains given by Eq. (1) are equated to zero and the resulting partial differential equations are integrated to yield:

$$\begin{aligned}u_1&=-a_1\frac{x}{r}-a_2\left(\frac{y^2}{2r}-\frac{x^2}{2r}\right)+a_3\frac{xy}{r}+a_4+a_6y\\v_1&=-a_1\frac{y}{r}+a_2\frac{xy}{r}-a_3\left(\frac{x^2}{2r}-\frac{y^2}{2r}\right)+a_5-a_6x\\w_1&=-a_1+a_2x+a_3y\end{aligned}\tag{3}$$

These displacement fields are due to the six components of the rigid body displacements and are represented in terms of the constants a_1 to a_6. If the element has six degrees of freedom for each of the three corner nodes, the displacement fields should be represented by 18 independent constants. Having used six constants for the representation of the rigid body modes, the remaining 12 constants are available for expressing the displacements due to the strains within the element. These constants can be apportioned among the strains in several ways. For the present element, the following is proposed:

$$\begin{aligned}\varepsilon_x&=a_7+a_8y\\&\quad-\frac{1}{r}\left(a_{15}\frac{y^2}{2}+a_{16}\frac{xy^2}{2}+a_{17}\frac{y^3}{6}\right)\\\varepsilon_y&=a_9+a_{10}x-\frac{1}{r}\left(a_{12}\frac{x^2}{2}+a_{13}\frac{x^3}{6}+a_{14}\frac{x^2y}{2}\right)\\\varepsilon_{xy}&=a_{11}\\k_x&=a_{12}+a_{13}x+a_{14}y\\k_y&=a_{15}+a_{16}x+a_{17}y\\k_{xy}&=a_{18}+\left(2a_{14}x+2a_{17}y\right)\end{aligned}\tag{4}$$

Eq. (4) is derived by first assuming the un-bracketed terms and adding the terms between brackets to satisfy the compatibility condition (Eq. (2)). It is then equated to the corresponding expressions in terms of u, v and w from Eq. (1) and the resulting equations are integrated to obtain:

$$\begin{aligned}u_2&=a_7x+a_8xy-a_{10}\frac{y^2}{2}+a_{11}\frac{y}{2}+a_{12}\frac{x^3}{6r}+a_{13}\frac{x^4}{24r}\\&\quad+a_{14}\frac{x^3y}{6r}-a_{16}\frac{y^4}{24r}+a_{18}\left(\frac{x^2y}{4r}-\frac{y^3}{12r}\right)\\v_2&=-a_8\frac{x^2}{2}+a_9y+a_{10}xy+a_{11}\frac{x}{2}-a_{14}\frac{x^4}{24r}\\&\quad+a_{15}\frac{y^3}{6r}+a_{16}\frac{xy^3}{6r}+a_{17}\frac{y^4}{24r}+a_{18}\left(\frac{xy^2}{4r}-\frac{x^3}{12r}\right)\\w_2&=-a_{12}\frac{x^2}{2}-a_{13}\frac{x^3}{6}-a_{14}\frac{x^2y}{2}-a_{15}\frac{y^2}{2}\\&\quad-a_{16}\frac{xy^2}{2}-a_{17}\frac{y^3}{6}-a_{18}\frac{xy}{2}\end{aligned}\tag{5}$$

The complete displacement functions for the element are obtained by adding the corresponding expressions for u, v and w from Eqs. (3) and (5). The translational degrees of freedom for the element are u, v, w. The three rotations about the x, y and z axes are given by:

$$\theta_x = \frac{\partial w}{\partial y} = a_3 - a_{14}\frac{x^2}{2} - a_{15}y - a_{16}xy - a_{17}\frac{y^2}{2} - a_{18}\frac{x}{2}$$

$$\theta_y = \frac{\partial w}{\partial x} = a_2 - a_{12}x - a_{13}\frac{x^2}{2} - a_{14}xy - a_{16}\frac{y^2}{2} - a_{18}\frac{y}{2}$$

$$\phi = \frac{1}{2}\left(\frac{\partial v}{\partial x} - \frac{\partial u}{\partial y}\right) = -a_2\frac{y}{r} + a_3\frac{x}{r} + a_6 - a_8x + a_{10}y - a_{14}\frac{x^3}{6r} - a_{16}\frac{y^3}{6r}6 - a_{18}\left(\frac{x^2}{4r} - \frac{y^2}{4r}\right) \tag{6}$$

The stiffness matrix $\boldsymbol{K}$ for the shell element is then calculated in the usual manner, i.e.,

$$\boldsymbol{K} = \left[\boldsymbol{C}^{-1}\right]^T \left\{\iiint \boldsymbol{B}^T \boldsymbol{D}\boldsymbol{B}\mathrm{d}v\right\}\left[\boldsymbol{C}^{-1}\right] \tag{7}$$

where, $\boldsymbol{B}$ and $\boldsymbol{D}$ are the strain and elasticity matrices, respectively, and $\boldsymbol{C}$ is the matrix relating the nodal displacements to the constant a_1 to a_{18}.

3. Consistent Load Vector

The simplest method to establish an equivalent set of nodal forces is the lumping process. An alternative and more accurate approach for dealing with distributed loads is the use of a consistent load vector which is derived by equating the work done by the distributed load through the displacement of the element to the work done by the nodal generalized loads through the nodal displacements. If a rectangular shell element is acted upon by a distributed load q per unit area in the direction of w, the work done by this load is given by:

$$P_1 = \int_{-a}^{a}\int_{-b}^{b} qw\mathrm{d}x\mathrm{d}y \tag{8}$$

where, a and b are the projected half length of the sides of the triangular element in the x and y directions, respectively. If w is taken to be represented by:

$$\{w\} = [\boldsymbol{N}^{\mathrm{T}}]\{a\} = [\boldsymbol{N}^{\mathrm{T}}][\boldsymbol{C}^{-1}]\{d\} \tag{9}$$

where, $\boldsymbol{N}^{\mathrm{T}}$ for the present element is given by (see Eqs. (3) and (5)):

$$\boldsymbol{N}^{\mathrm{T}} = [-1, x, y, 0, 0, 0, 0, 0, 0, 0, 0, -\frac{x^2}{2}, -\frac{x^3}{6}, -\frac{x^2y}{2}, -\frac{y^2}{2} - \frac{xy^2}{2} - \frac{y^3}{6} - \frac{xy}{2}]$$

$\{a\}$ is the vector of the independent constants, $[\boldsymbol{C}^{-1}]$ is the inverse of the transformation matrix and $\{d\}$ is a vector of the nodal degrees of freedom. The work done by the consistent nodal generalized force through the nodal displacements $\{d\}$ is given by:

$$P_2 = \{\boldsymbol{F}\}^{\mathrm{T}}\{d\} \tag{10}$$

Hence, from Eqs. (8)-(10), the nodal forces are obtained, i.e.:

$$\{\boldsymbol{F}\} = \int_{-a}^{a}\int_{-b}^{b} q\left|\boldsymbol{N}^{\mathrm{T}}\right|\left[\boldsymbol{C}^T\right]\{a\}\left[\boldsymbol{N}\right]^{-1}\mathrm{d}x\mathrm{d}y \tag{11}$$

Eq. (11) gives the nodal forces for a single element; and the nodal forces for the whole structure are obtained by assembling the elements' nodal forces.

4. Problems Considered

4.1 Spherical Cap Subjected to a Point Load

The geometry of the spherical shell considered in this section is shown in Fig. 2. The shell is simply supported on the boundaries of a square plan form such that the normal displacement is zero along the edges, while the in-plane displacements normal to the edges are freely allowed to take place. The shell has the following dimensions and elastic properties: $a = b$ = 400 mm, r = 2,400 mm, t = 2.54 mm, E = 7,037 kg/mm^2 and ν = 0.3. It is subjected to a point central load p = 45.4 kg. The symmetry of the shell and loading allows consideration of a quadrant of the shell to be analyzed.

This spherical cap was analyzed previously by Gallagher [19] using a rectangular shell finite element with linear membrane displacement function for u, v and w.

Yang [7] has solved this problem by using a rectangular finite element, where all the displacement components are represented by cubic polynomials and also proposed a series (closed form) solution. Later on, Dawe [8] used a quintet order triangular element, having 54 degrees of freedom to analyze the same shell. He reported that the results obtained were more accurate than those given by Yang [7] for the same number of elements. However, this element has an excessively large number of degrees of freedom, which would require large computational effort to perform the analysis using this element. In comparison, the present element includes only six degrees of freedom.

The spherical shell described above is analyzed here using: the triangular spherical shell element that has only five degrees of freedom at each corner node, which is given in Ref. [17]; and the rectangular spherical shell element developed in the current study. The results from both analyses are compared together and with those obtained from the series (closed form) solution given by Yang [7].

Convergence tests were carried out for the normal deflection at the centre of the shell. Fig. 3 shows that both elements require only 6 × 6 mesh size to converge

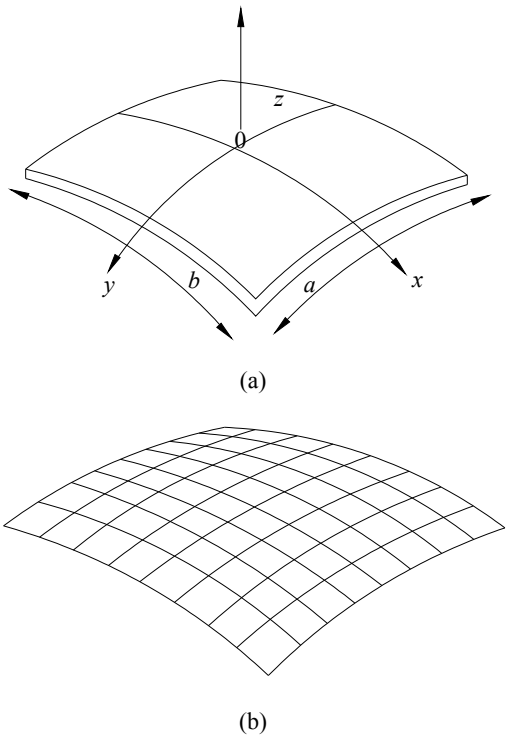

(a)

(b)

Fig. 2 Spherical cap: (a) shell geometry; (b) 8 × 8 mesh.

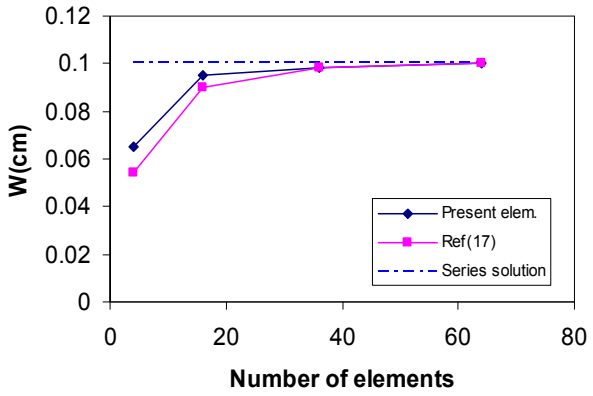

Fig. 3 Convergence of *W* at the Center.

to acceptable results with a difference of less than 3% in the case of the triangular element developed by Sabir and Djoudi [17] and less that 2.2% in the case of present element compared with the series solution, while it was reported that Gallagher element [19] gives an error of more than 10% for the same mesh size. Further investigations on the deflection are shown in Fig. 4, which indicates excellent agreement between the results obtained from the present element and the series solution for the variation for normal deflecting along a centre line.

The direct stress resultant, N_x, and the bending moment, M_x, are computed along the centre line "ox" in the x direction. The results obtained from the (8 × 8) meshes are presented in Figs. 5 and 6 for N_x and M_x, respectively. The results obtained from the series solution are also shown in the figures for comparison. It is noted that the results for the membrane stress resultants agree well with those obtained from the series solution.

These results clearly show that the response of spherical shell can be adequately analyzed using a reasonable number of elements to obtain convergence of deflection and stresses. The results also confirm the suitability of the proposed triangular shell element for the analysis of spherical shell roof structures in the form of a polygon shaped. This form of structure is often used by architects to roof exhibition halls and public buildings. The authors found that one of this type of roof was implemented in the field. To the knowledge of the authors, no known solution to this problem is available in the published literature.

4.2 Analysis of Spherical Polygon Shaped Shell Roof

The spherical shell roof structure considered is shown in Fig. 7. It has a central rise above the cornered supports of 4.0 m and a total horizontal span between each of the two diagonally opposite supports of 18 m. It is spherical in form having a radius of curvature of 12.125 m in each of the principle directions x and y and a thickness of 100 mm. The Young's modulus of the shell material, $E = 2 \times 10^9$ kg/cm^2 and its Poisson's ratio, $\nu = 0.3$. The dimensions are shown in Fig. 7. The polygon shaped roof is loaded by a normal uniformly distributed load of 500 kg/m^2 and it is assumed to be fixed to rigid supports at all four end corners.

Due to symmetry and uniform loading, only one quadrant of the shell is analyzed. The conditions for symmetry along the centre line require that the in-plane displacements and rotations normal to the plane of symmetry are zero.

Two models (shown in Fig. 8) are used to examine the effect of the mesh size needed for the analysis of one quarter of the shell on the calculated deflections and stresses. In the first model, a moderate mesh 12 × 12 mesh size is considered (Fig. 8a), while the second model considered a finer mesh of 18 × 18 mesh size (Fig. 8b).

The analysis was performed and the quantities

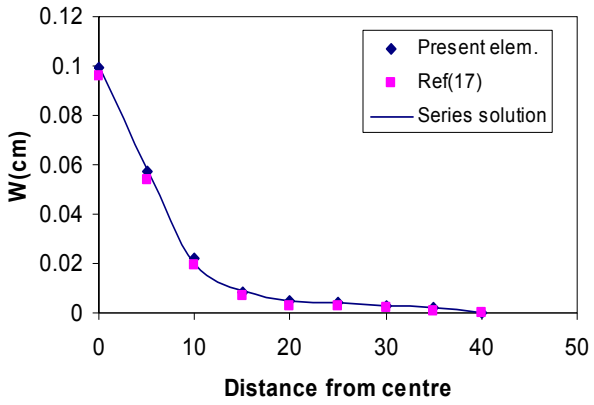

Fig. 4 Variation of *W* along "ox".

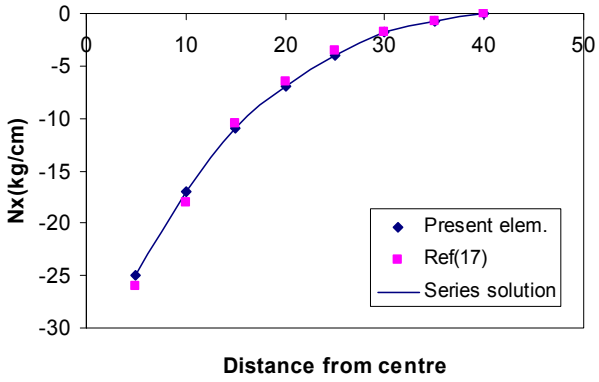

Fig. 5 Variation of *Nx* along the center line.

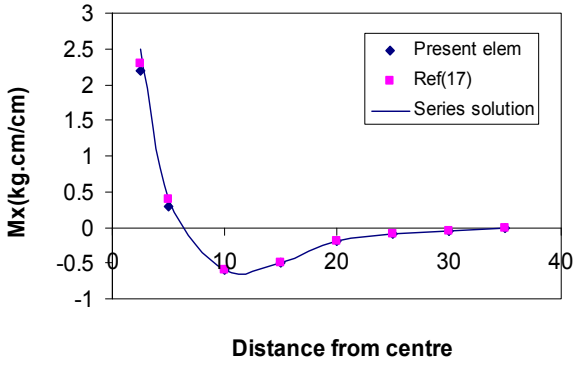

Fig. 6 Variation of M_x along the center line.

necessary for design are calculated including the normal deflections, the direct membrane stress resultants in the y and x directions as well as the bending stress resultant M_x along the central line ox. Fig. 9 shows the distribution of the normal deflections of the roof. The hoop stress, N_y, and the direct stress, N_x, are presented in Figs. 10 and 11, respectively. Fig. 12 displays the bending stress resultant, M_x.

Fig. 9 shows that the normal deflection along ox is almost constant and downward throughout the central portion of the shell. Thereafter, the deflection decreases and becomes upward reaching a maximum of almost the same magnitude as the downward deflection at the centre of the shell. The deflection decreases over the last portion of the shell until it becomes zero at the corner support.

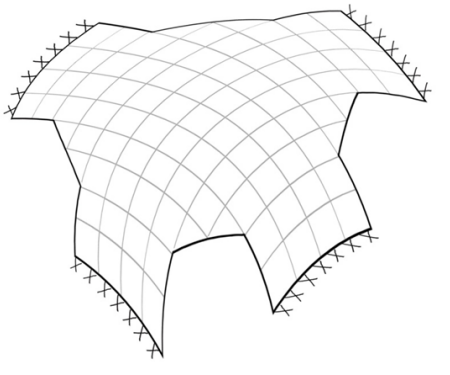

(a)

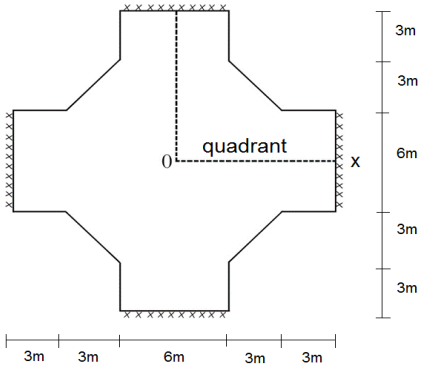

(b)

Fig. 7 Polygon shaped spherical shell roof: (a) roof geometry; (b) plan view.

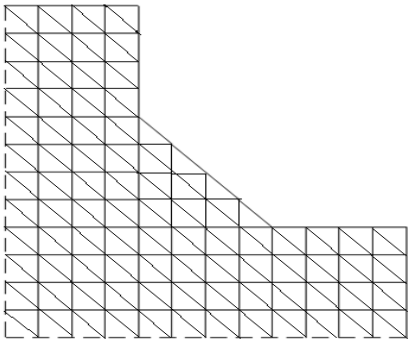

(a)

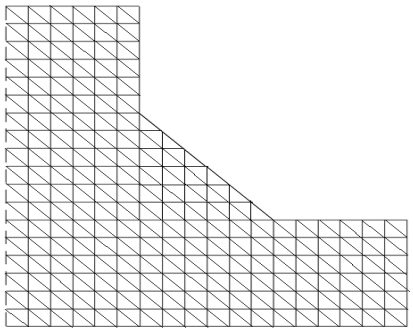

(b)

Fig. 8 Configuration of mesh used in the analyses: (a) a moderate mesh; (b) fine mesh.

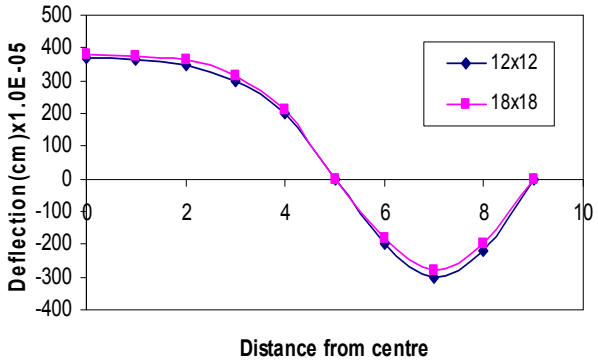

Fig. 9 Radial deflection along ox.

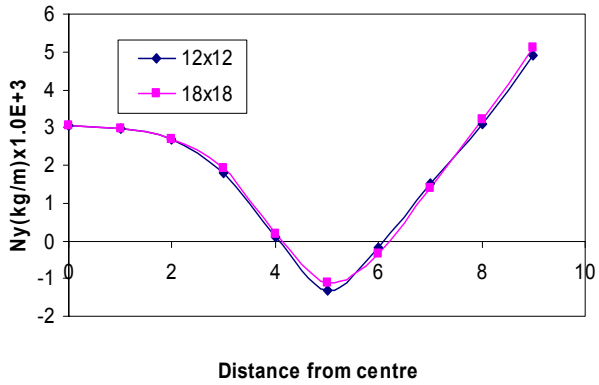

Fig. 10 Hoop stress N_y along ox.

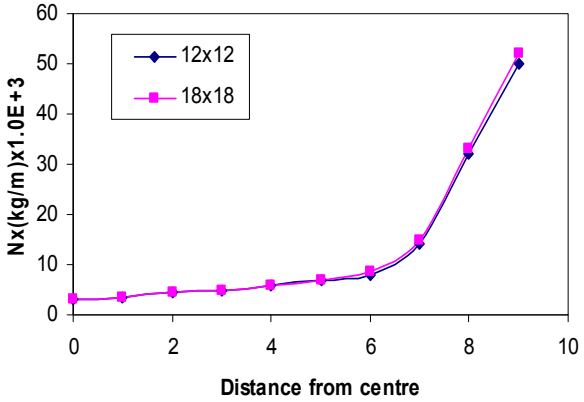

Fig. 11 Direct stress N_x along ox.

Fig. 10 shows that the hoop stress resultant N_y is compressive over the central part and at the support along ox, but becomes tensile over a small length between the two regions. On the other hand, the direct stress resultant N_x increases steadily at a small rate along ox over the central region but increases rapidly over the region near the support, as shown in Fig. 11. This behavior is consistent with the membrane theory, which gives an almost constant stress resultant N_x in the central region (near the crown) and then increases rapidly towards the support. It is also noted from Figs. 10 and 11 that the magnitude of the maximum stress resultant N_x is much larger (one order of magnitude) than the maximum of the hoop stress, N_y.

Fig. 12 shows that the bending stress resultant M_x along ox is generally small in the central region, for a

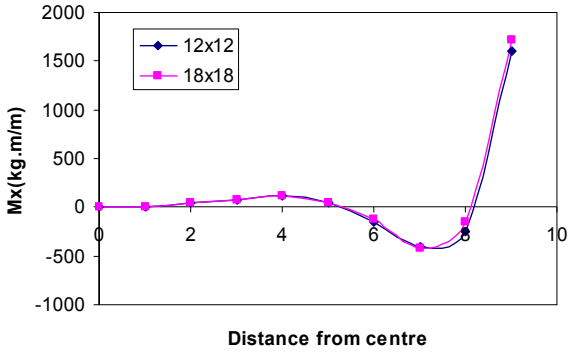

Fig. 12 Bending moment M_x along ox.

length of about two thirds of the span. Afterwards, it changes sign for a small length but increases sharply towards the support with a maximum value at the fixed support, as expected.

All the above figures show clearly that, for all practical purposes, the results obtained from the two models do not differ significantly, confirming again the efficiency of the developed element. However, the fine mesh was used in the following section.

4.3 Polygon Shaped Shell with Circular Arched Beam Stiffeners

In practice, shells having large spans are stiffened by beams. To investigate the effect of such stiffening beams on the deflections and stresses, the case of cross shaped roof structure stiffened by arched beams spanning between two diagonally opposite supports is considered. To investigate the effect of the depth of the diagonal arched beam stiffeners on the resulting deflections and stresses, two cases were considered H = 200 mm and 400 mm, while the width, B is kept at 200 mm. The layout and geometry of the problem considered are shown in Fig. 13.

The developed strain–based rectangular spherical element is used in the analysis of the spherical shell and the diagonal arched beams are idealized by a six nodal degrees of freedom beam element. The stiffness matrix of the beam is based on cubic variation of both the vertical and horizontal displacements and linear variation of the axial displacement and the angle of twist. Thus, the beam element and the strain-based triangular element have the same degrees of freedom and complete compatibility is ensured when these elements are used in the assembly of the overall structural matrix.

After assembling the global stiffness matrix and establishing the load vector using Eq. (11), the derived equilibrium equations were solved and the response was obtained. The results reported here include the normal deflections, the direct membrane stress resultants in the y and x directions as well as the bending stress resultant M_x along the central line ox. Fig. 14 shows the distribution of the normal deflections of the roof. The hoop stress, N_y, and the direct stress, N_x, are presented in Figs. 15 and 16, respectively. Fig. 17 displays the bending stress resultant, M_x.

Fig. 14 shows that the stiffeners resulted in significant reduction of roof deflections. For example, the maximum deflection (at the centre) decreased by 65% for the shallow beam and 80% for the deeper beam case, compared with the case of the shell having no stiffeners. In addition, the shell stress resultants decreased significantly. For example, Fig. 15 shows that the direct stress resultant N_y has decreased by about 33% and 66%, for the cases of H = 200 mm and H = 400 mm, respectively. Similar observations can be made from Fig. 16 with regard to the direct stress resultant N_x along ox. Likewise, the bending stress, M_x, has been reduced significantly due to the use of the stiffeners as shown in Fig. 17. A reduction of about 30% is achieved with the thinner beam and about 60% with the thicker beam.

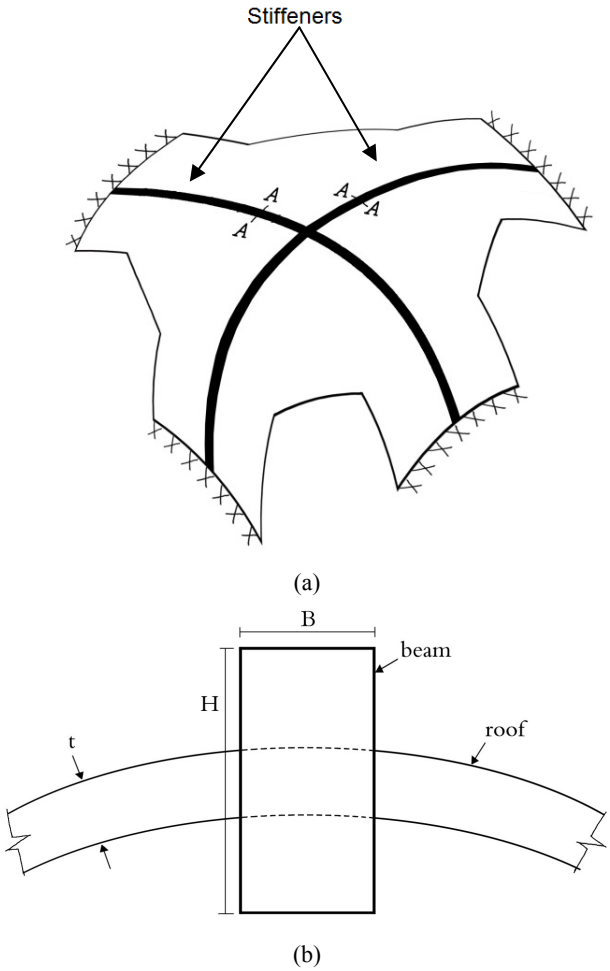

Fig. 13 Polygon shaped spherical shell with stiffening beams: (a) the roof with stiffeners; (b) Section A-A.

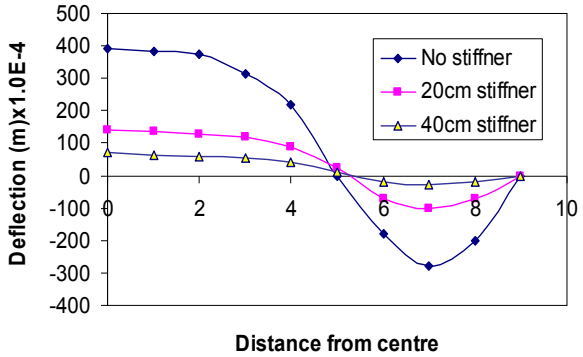

Fig. 14 The effect of stiffeners on the deflection along the center line "ox".

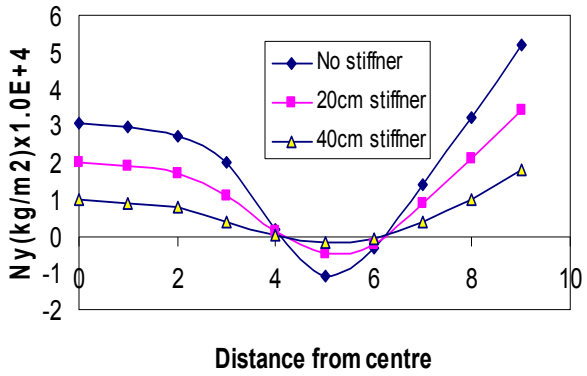

Fig. 15 The effect of stiffeners on (ny) along the center line "ox".

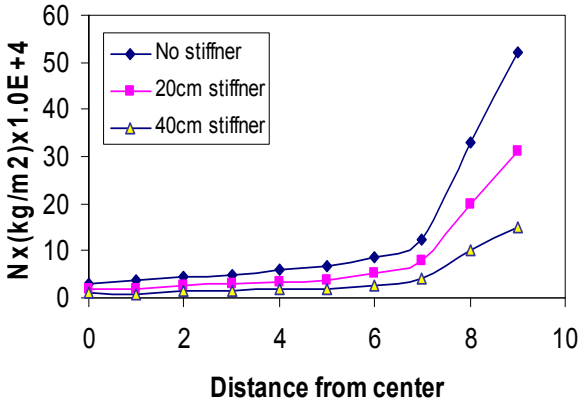

Fig. 16 the effect of stiffeners on (N_x) along the center line "ox".

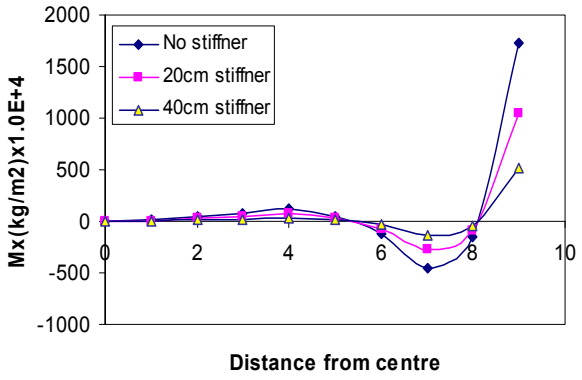

Fig. 17 The effect of stiffeners on (M_x) along the center line "ox".

5. Conclusions

A new spherical shell triangular strain-based finite element was developed using shallow shell formulations. The element has six degrees of freedom at each corner node, the essential five external degrees of freedom as well as an additional sixth degree of freedom representing the in-plane rotation. The element is therefore fully compatible with and can be used in conjunction with arched beam elements having all the essential six degrees of freedom.

The element was verified and validated through the analysis of a simply supported square spherical shell problem subjected to concentrated load, and comparing the results with the predictions of other approaches. The results of the analysis showed that

reasonably accurate results were obtained even modeling the shells using fewer elements compared to other shell element types.

The developed element was then used in a finite element model to analyze the response of polygon shaped spherical roof structure. The distribution of normal deflection and the various components of stresses are evaluated. The results showed that this type of shell roof exhibits large deflections at the centre and large stresses at the corners because of its non uniform shape and supporting conditions. The response of the roof stiffened using diagonal arched beams was also analyzed. The diagonally lined stiffeners were found to considerably reduce the deflections and stresses of cross shaped spherical roof structures.

References

[1] Grafton, P. E., and Strome, D. R. "Analysis of Ax Symmetric Shells by the Direct Stiffness Method." *AIAA* 1 (1): 2342-7.

[2] Jones, R. E., and Strome, D. R. 1966. "Direct Stiffness Method Analysis of Shells of Revolution Utilizing Curved Elements." *AIAA* 4: 1519-25.

[3] Brebbia, C., and Connor, J. J. 1967. "Stiffness Matrix for Shallow Rectangular Shell Element." *J. Eng. Mech. Div. ASCE* 93 EMS: 43-65.

[4] Cantin, G., and Clough, R. W. "A Curved Cylindrical Shell Finite Element." *AIAA Journal* 6: 1057-62.

[5] Sabir, A. B., and Lock, A. C. "A Curved Cylindrical Shell Finite Element." *Int. J. Mech. Sci.* 14: 125.

[6] Cowper, G. R., Lindberg, G. M., and Olson, M. D. "A Shallow Shell Finite Element of Triangular Shape." *Int. J. Solids and Structures* 6: 1133-56.

[7] Yang, T. Y. 1973. "High Order Rectangular Shallow Shell Finite Element." *J. Eng. Mech. Div. ASCE* 99 EM1: 157.

[8] Dawe, D. J. 1975. "High Order Triangular Finite Element for Shell Analysis." *Int. J. Solids Structures* 11: 1097-110.

[9] Ashwell, D. G., and Sabir, A. B. "A New Cylindrical Shell Finite Element Based on Simple Independent Strain Functions." *Int. J. Mech. Sci.* 14: 171-83.

[10] Sabir, A. B., and Charchaechi, T. A. 1982. "Curved Rectangular and General Quadrilateral Shell Finite Elements for Cylindrical Shells." *The Math. of Finite Element and Appli.* IV: 231-9.

[11] Sabir, A. B., and Ramadhani, F. 1985. "A Shallow Shell Finite Element for General Shell Analysis." *Variation Method In Engineering Proceedings of The 2nd International Conference,* University of Southampton. England.

[12] Sabir, A. B., and Djoudi, M. S. 1990. "A Shallow Shell Triangular Finite Element for the Analysis of the Analysis of Hyperbolic Parabolic Shell Roof." *FEMCAD, Struct. Eng. and Optimization,* 49-54.

[13] Mousa, A. I. 1998. "Finite Element Analysis of a Gable Roof." *Computational Structural Engineering in Practice* 6 (7): 256-68.

[14] Mousa, A. I., and Kameshki, E. 2017. "Strain Based Finite Element for Analysis of Cylindrical Shell Dam." *American Journal of Engineering Research* 6 (2): 119-28.

[15] Mousa, A. I., and Sabir, A. B. 1994. "Finite Element Analysis of Fluted Conical Shell Roof Structures." *Computational Structural Engineering in Practice* 6 (2): 173-81.

[16] Sabir, A. B. 1997. "Strain Based Shallow Spherical Shell Element." In *Proc. Int. Conf on the Math. Finite elements and application,* Brunel University, England.

[17] Sabir, A. B., and Djoudi, M. S. 1998. "A Shallow Shell Triangular Finite Element for the Analysis of Spherical Shells." *Structural Analysis J.,* PP51-57.

[18] Mousa, A. I., and Djoudi, M. S. 2015. "A Shallow Shell Finite Element for the Linear and Nonlinear Analysis of Spherical Shells." *International Journal of Civil and Environmental Engineering* 15 (5): 24-9.

[19] Gallagher, R. H. 1966. "The Development and Evaluation of Matrix Methods for Thin Shell Structural Analysis." Ph.D. thesis, State University of New York Buffalo.